Stability Analysis of a Networking DC Microgrid with Distributed Droop Control and CPLs

Marco Carnaghi, Paula. Cervellini, Marcos Judewicz, Rogelio Garcia Retegui and Marcos A. Funes

***Abstract*—Networking direct current microgrids (DCMGs) have gained interest in the pursuit of achieving higher integration of renewable energy sources (RESs) and improving system resilience and reliability. The highly cooperative nature of these MGs is an advantage in order to maximize the RESs utilization and minimize grid power demand. However, ensuring stable and robust operation in the presence of significant load fluctuations constitutes a major challenge. Overvoltages and overcurrents, among other phenomena related to system stability, deteriorate the power quality and can be prevented with proper analysis. In this regard, numerous research studies have presented proposals related to the achievment of an optimal power distribution among the individual MGs of a networking DCMG. However, the stable operation of these MGs still requires further analysis to reach the same level of understanding accomplished in other topologies. Therefore, in this paper, a stability analysis for a networking DCMG is presented. This analysis includes the modeling of the system considering a distributed control strategy and the presence of uncertain active loads, and the subsequent formulation of sufficient conditions of load and generation power for robust stability of the DCMG. Finally, the concordance between the results of the circuital simulations and those related to the stability analysis is assessed. Moreover, conclusions about the representation of the microgrid and the optimal tuning of the controller´s gains and parameters are drawn.**

***Index Terms*—DC microgrid, Networking microgrid, Constant power load, Adaptive droop control, Robust Stability, Power electronics**

I. Introduction

Interest in DCMGs has expanded rapidly in the last few years in search of an integrative, efficient, sustainable, and reliable solution for distributed generation systems. DCMGs are direct current networks with locally-controlled DC generation nodes (GNs), such as storage systems with its associated power converters, and passive and active loads. As many distributed generators, storage systems and appliances are inherently DC, their interconnection through a DCMG enhances the system efficiency [1]–[3]. DCMGs are implemented considering different topologies [4], some of which are shown in Fig. 1. In a single-bus topology, the GNs and loads are connected to a single bus through power converters. This structure is commonly employed in low voltage applications such as residential complexes and telecom systems [1], [5]–[7]. The ring bus structure is more robust against faults in the power converters, and it has been used in distributed renewable and storage plants [8], [9]. The networking DCMG topology is characterized by being organized into groups, which are constituted by spatially close connected GNs and loads, which are then interconnected by the main DC bus [4]. This topology is commonly found in data centers, universities, and technology institutions [4], [10]–[13]. Networking DCMGs represent a novel trend in smart distribution grids, aiming to maximize renewable energy sources utilization, reduce the power demand from the utility grid, and enhance overall reliability [11], [14]–[16]. Due to their resource-sharing-based approach, which improves adaptability and resilience, networking DCMG is chosen as the topology of interest for the analysis presented in this paper.

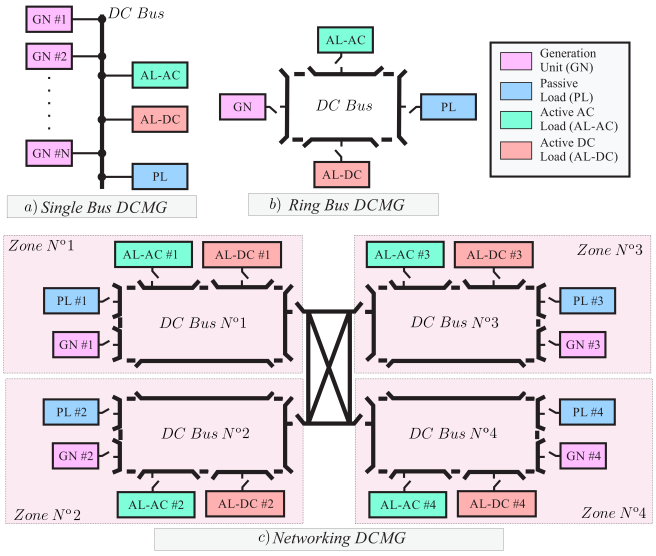

Fig. 1. DCMG topologies: Single Bus DCMG, Ring Bus DCMG and Networking DCMG.

The nature of this type of DCMG is strongly cooperative, therefore, distributed control systems are commonly considered as a better approach than centralized strategies. These systems rely on coordination and consensus to achieve two main objectives: DC bus voltage regulation and proportional load sharing among the GNs, with the goal of avoiding overloading any of the GNs under nominal demand [1], [5], [11]. However, the dynamics of the controllers interact with each other and with loads that vary substantially over time, which, in turn, may compromise the stability of the DCMG [1], [17]. Furthermore, the stability issue has been identified in the literature as a problem of great relevance [18], [19]. Stable and robust operation is crucial to prevent

This work was supported in part by the Universidad Nacional de Mar del Plata (UNMDP), the Consejo Nacional de Investigaciones Científicas y Tecnológicas (CONICET) PIP11220200102643CO and by the Agencia Nacional de Promoción Científica y Tecnológica (ANPCYT), Argentina.
[e-mail:mcarnaghi@fi.mdp.edu.ar; paulacervellini@fi.mdp.edu.ar; marcosj@fi.mdp.edu.ar; rgarcia@fi.mdp.edu.ar; mfunes@fi.mdp.edu.ar]

overvoltages, overcurrents, and other bus voltage fluctuations that deteriorate the power quality and can potentially damage users equipment [16].

Different stability analyses of DCMGs have been proposed in the literature, but most of them are limited in their applicability to networking DCMGs given that the considerations made in them are oriented to DCMGs with different topologies and, therefore, different characteristics [5], [20]–[23]. While many publications on networking DCMGs focus on consensus strategies for global power distribution, stable and robust operation of these systems has not been widely addressed [11], [24], [25]. In a previous study [26], a scenario considering multiple GNs and multiple CPLs is presented, and the stability of the system is evaluated using a LMI formulation and a polytopic space, which can handle microgrids with multiple PCCs. While the topology studied in [26] is compatible with a networking DCMG, the control strategy associated with the GNs is based on a static droop control, which is not suitable for a networking DCMG. As networking DCMGs are strongly cooperative in nature, not considering any distributed control strategy in the analysis results in the loss of this key feature. Moreover, the impact of the controller's interactions on the system stability is neglected as GNs with a static droop control act as autonomous entities. Therefore, further study is needed to evaluate the impact of distributed control strategies on the stable operation of networking DCMGs.

In this paper, a stability analysis focusing on networking DCMGs is presented. In order to carry out the mentioned analysis a model based on well known space state modeling techniques is introduced, where spatially-closed GNs and loads connected to the same local DC bus are grouped into units. The model also considers a distributed control strategy where each GNs has an adaptive droop controller whose set points are defined from the consensual control layer. Then, by using the presented model, sufficient conditions of load power consumption and local DC bus voltages for robust stability of networking DCMGs are obtained by means of convex polytopic modeling theory and Hurwitz stability. Furthermore, the presented formulation is employed to gain insights into the impact of controller gains and parameters on stability. The latter allows to identify how to modify the parameters in order to improve stability.

The rest of the paper is organized as follows: in Section 2, the model of the networking DCMG is developed. Sufficient conditions for robust stability are obtained in Section 3. Simulation results are presented in Section 4. Finally, conclusions are summarized in Section 5.

II. Networking DC Microgrid Model

The networking DCMG model involves: presenting the microgrid bus representation, finding the expressions that describe the circuit and control dynamics of local models, and building the overall model by applying graph theory to model the topology of the microgrid [24], [27].

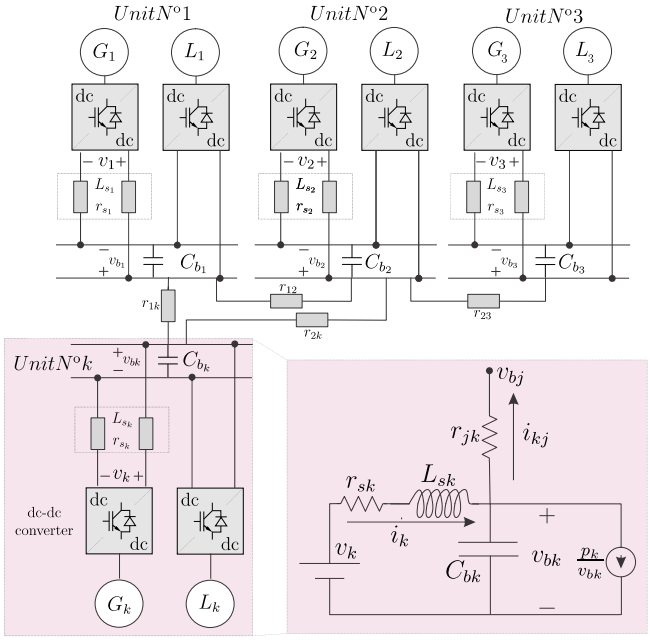

Fig. 2. Proposed DCMG model based on multi-unit scheme.

A. Networking microgrid bus representation

As shown in Fig. 2, the microgrid is considered to be constituted by the interconnection of different units. Each unit covers GNs and loads that are spatially-closed connected. In particular, these units include:

- DC power converter in voltage mode represented by a controllable voltage source (v_k), which operates as the interface between the DC bus and a dispatchable source (G_k) such as a battery or the DC bus in a two stages scheme.
- The connection impedance between the converter outputs and the k^{th} local DC bus, which is constituted by an inductance (L_{sk}) and a resistance (r_{sk}).
- DC-link capacitance of the k^{th} unit (C_{bk}).
- Resistive interconnection impedance (r_{jk}) between j^{th} and k^{th} bus.
- A CPL represented by a current source p_k/v_{bk}, i.e, the control is assumed to be working on the constant power region, thus, avoiding saturation of the duty-cycle [17].

Then, the interconnections among the units is defined according to the topology of the DCMG.

B. Dynamic Model of the k-unit

The dynamic model of each individual unit is determined by combining the model of the control loop of the DC power converter and its output circuit, which includes L_{sk}, r_{sk}, C_{bk} and the load.

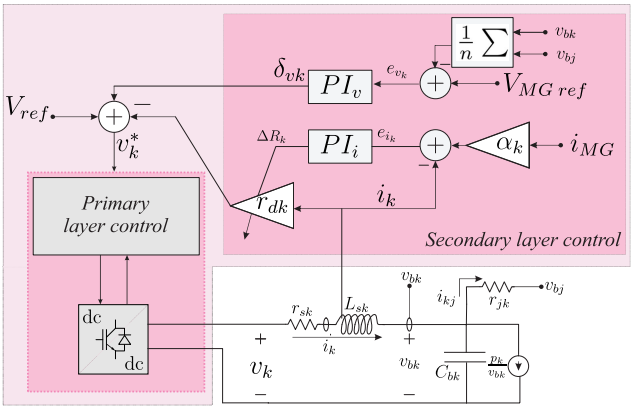

Fig. 3. k^{th}-unit model.

1) Control loop model: Fig. 3 shows the voltage controller of the DC power converter, which consists of two layers: a primary layer control composed of an inner current and outer voltage control loop, and an external secondary layer control corresponding to an adaptive droop control scheme that defines the voltage reference v_k^* for the primary layer control. The primary layer control is supposed to have much higher dynamics than the secondary layer control, so it is possible to assume that $v_k \approx v_k^*$. For the secondary layer control, different adaptive droop control schemes have been proposed in the literature, where the main difference is whether the control adapts the voltage reference [6], the droop resistance [28] or both [29]. In this paper, the scheme proposed in [29] is considered because it includes not only adaptive droop resistance but also consensus operation. Then, the following expressions can be deduced for the control variables:

$$v_k = v_k^* \tag{1}$$
$$v_k^* = V_{ref} + \delta_{v_k} - r_{d_k} * i_k \tag{2}$$
$$r_{d_k} = r_{d0_k} + \Delta r_k \tag{3}$$
$$\dot{\delta}_{v_k} = \dot{e}_{v_k} * K_{pv\,k} + e_{v_k} * K_{iv\,k} \tag{4}$$
$$(\Delta \dot{r}_k) = \dot{e}_{i_k} * K_{pi\,k} + e_{i_k} * K_{ii\,k} \tag{5}$$
$$e_{v_k} = V_{MG\,ref} - v_{MG},\ e_{i_k} = i_k - \alpha_k * i_{MG} \tag{6}$$

where v_k and i_k are output voltage and current of the source side converter. While, r_{d_k}, r_{d0_k} and Δr_k are the total, constant and varying terms of the droop resistance, which is modulated to achieve current sharing among the GNs. In this sense, a fraction ($\alpha_k = I_{rated\,k} / \sum_{j=1}^{n} I_{rated\,j}$) of the total current load ($i_{MG} = \sum_{j=1}^{n} \frac{p_j}{v_{bj}}$, where n is the number of units considered in the DCMG) is assigned to each GN [29]. For its part, δ_{v_k} refers to the voltage reference adjustment defined to ensure convergence of the average bus voltage of the DC microgrid ($v_{MG} = \frac{1}{n}\sum_{j=1}^{n} v_{bj}$, with v_{bk} the voltage across the DC-link capacitor of the $k-th$ bus C_{bk}) to the setpoint defined by V_{ref} and V_{MGref}. The variable V_{ref} represents the nominal setpoint value for the output voltage of each DC converter, while $V_{MG;ref}$ represents the setpoint value for the average DC bus voltage. In more complex control systems with multiple layers, these reference variables may be defined by higher control hierarchies. However, for the purposes of the present analysis, it is assumed that these reference values are constant because their variations are expected to be slower than the dynamics of the adaptive droop controllers. Lastly, e_{v_k} and e_{i_k} are the voltage and current errors, respectively; and $K_{pv\,k}$, $K_{iv\,k}$, $K_{pi\,k}$ and $K_{ii\,k}$ are the PIs controllers gains.

2) Output circuit model: To describe the interconnections among the units, an undirected graph is defined by $\beth = (\vartheta, \xi)$ where each element in the vertex set ϑ represents one DC microgrid unit, and each element of the edge set ξ represents one transmission line between two different units. In other words, if $(k, j) \in \xi$, j^{th} unit and k^{th} unit are neighbors. Thus, in the following expressions, $\aleph_k$ has the indices of neighboring units to the k^{th} unit [27]. Then, the following expressions for the output circuit are deduced according to Fig. 3:

$$L_{sk}\dot{i}_k = v_k - v_{bk} - i_k * r_{sk} \tag{7}$$
$$C_{bk}\dot{v}_{bk} = i_k - \frac{p_k}{v_{bk}} - \sum_{j=1, j\neq k, j\in\aleph_k}^{n} i_{jk} \tag{8}$$
$$i_{jk} = \frac{v_{bk} - v_{bj}}{r_{jk}} \tag{9}$$

where i_{jk} is the current in the transmission line between k^{th} and j^{th} units. The current injection into the CPL is $\frac{p_k}{v_{bk}}$. Note that, as the set $\aleph$ represents the interconnections among the units, the single-bus and ring-bus topologies turn to be particular cases where each unit is simply connected to its single or two adjacent units.

3) k-unit dynamic model: From previous expressions, the following state equations are deduced,

$$L_{sk}\dot{i}_k = V_{ref} + \delta_{v_k} - v_{bk} - i_k * (r_{sk} + r_{d0\,k}) + (-\Delta r_k * i_k) \tag{10}$$

$$C_{bk}\dot{v}_{bk} = i_k - \frac{p_k}{v_{bk}} - \sum_{j=1, j\in\aleph_k}^{n} \frac{v_{bk} - v_{bj}}{r_{jk}} \tag{11}$$

$$\begin{aligned}(\Delta \dot{r}_k) = {} & \frac{K_{pi_k}}{L_{sk}} * V_{ref} + [K_{ii_k} - \frac{K_{pi_k}}{L_{sk}} * (r_{d0\,k} + r_{sk})] * i_k \\ & - \frac{K_{pi_k}}{L_{sk}} * v_{bk} + \frac{K_{pi_k}}{L_{sk}} * \delta_{vk} + \frac{K_{pi_k}}{L_{sk}} * (-\Delta r_k * i_k) \\ & + K_{pi_k} * \alpha_k * \sum_{j=1}^{n} (-\frac{d}{dt}(\frac{p_j}{v_{bj}})) \\ & + \alpha_k * K_{ii_k} * \sum_{j=1}^{n} -\frac{p_j}{v_{bj}}\end{aligned} \tag{12}$$

$$\begin{aligned}\dot{\delta}_{v_k} = {} & K_{iv_k} * V_{MG\,ref} - \frac{K_{iv_k}}{n}[\sum_{j=1}^{n} v_{bj}] - \frac{K_{pv_k}}{n}[\sum_{j=1}^{n} \frac{i_j}{C_{bj}}] \\ & - \frac{K_{pv_k}}{n}[\sum_{j=1}^{n} -\frac{p_j}{v_{bj} * C_{bj}}]\end{aligned} \tag{13}$$

where the three nonlinear terms present in the model refer to:$-\frac{p_j}{v_{bj}}$, $\frac{d}{dt}(\frac{p_j}{v_{bj}})$ and $(-\Delta r_k * i_k)$. The equations presented show how the microgrid variables v_{bk} and i_k are affected by control variables Δr_k and δ_{v_k}.

C. Overall model

The overall model is obtained by combining the individual models of the microgrid units, with the goal of accurately representing the dynamics of the microgrid.

Let $I \in \Re^n$, $V_b \in \Re^n$, $\Delta_v \in \Re^n$, $\Delta r \in \Re^n$, $P \in \Re^n$, $V_{REF} \in \Re^2$, $X \in \Re^{4n}$ and nonlinear functions $h(.,.) : \Re^n x \Re^n \to \Re^n$ and $g(.,.) : \Re^n x \Re^n \to \Re^n$ be:

$$\begin{aligned} I &= [i_1, ..., i_n]^T,\ V_b = [v_{b1}, ..., v_{bn}]^T \\ \Delta_v &= [\delta_{v_1}, ..., \delta_{v_n}]^T,\ \Delta r = [\Delta r_1, ..., \Delta r_n]^T \\ V_{REF} &= [V_{ref}, V_{MG\ ref}]^T \\ X &= [I^T, V_b^T, \Delta_v^T, \Delta r^T]^T,\ P = [p_1, ..., p_n]^T \\ H &= h(p, v_b) = [-\frac{p_1}{v_{b1}}, -\frac{p_2}{v_{b2}}, ..., -\frac{p_n}{v_{bn}}]^T \\ G &= g(\Delta r, i) = [-\Delta r_1 * i_1, -\Delta r_2 * i_2, ..., -\Delta r_n * i_n]^T \end{aligned}$$

Then, with the above definitions, the overall microgrid model can be written as:

$$\dot{x} = Ax + BV_{REF} + MG + CH + E\dot{H} \tag{14}$$

where the matrices $A \in \Re^{4n} x \Re^{4n}$, $B \in \Re^{4n} x \Re^{2n}$ and $M \in \Re^{4n} x \Re^n$, $C \in \Re^{4n} x \Re^n$, and $E \in \Re^{4n} x \Re^n$. In order to build these matrices, previous expressions and the definition of the state variables vector X as $x_k = i_k$, $x_{n+k} = v_{bk}$, $x_{2n+k} = \delta v_k$ y $x_{3n+k} = \Delta r_k$, are considered. Note that (14) is also applicable for DC microgrids with multiple GNs or without them and with or without loads. For example, in presence of RESs operating in MPPT mode, i.e., working as constant power sources (CPS), they can be modeled as presented for CPLs, but with inverted power flow [17].

III. Robust stability analysis

In this section, a robust stability framework for the system presented in (14) is developed. This formulation allows a straightforward evaluation of the system stability over a given range of operation from a set of finite, reduced and clearly defined conditions. In the present article, the considered range of operation for the system is defined on the basis of the value range contemplated for the bus voltages and the power demanded by the CPLs in each unit. This analysis has been carried out combining concepts from uncertainties characterization theory [30], [31] and robust stability [32], [33]. In particular, in this paper, uncertainties are characterized through the theory of polytopic sets [30], and subsequently those concepts are applied to robust stability conditions.

In the first place, the uncertain power demanded by the CPLs is expressed as a bounded polytopic set $\check{P}$ given by,

$$\check{P} = \{p : p_k \in [\underline{p_k}, \overline{p_k}], k = 1, ..., n\} \tag{15}$$

where $\underline{p_k}$ and $\overline{p_k}$ represent the minimum and maximum values of the power demanded by the k^{th} CPL, respectively.

Similarly, the set of DC bus voltage setpoints for steady-state operation of the DCMG is defined as,

$$\nu_b^{eq} = \{V_b^{eq} \in \mathbb{R}^n : v_{bk}^{eq} \in [\underline{v_{bk}}, \overline{v_{bk}}], k = 1, ..., n\} \tag{16}$$

where $\overline{v_{bk}} > \underline{v_{bk}} > 0$ represent the maximum and minimum bounds of the DC bus voltage setpoints during steady state operation.

Once $\check{P}$ and ν_b^{eq} are defined, it is possible to express the set of feasible equilibria of the system as:

$$\chi^{eq} = \chi^{eq}(\check{P}, \nu_b^{eq}) \tag{17}$$

$$\begin{aligned} \chi^{eq} = \{&x^{eq} \in \mathbb{R}^{4n} : \\ &A.x + B.V_{REF} + M.G + C.H + E.\dot{H} = 0, \\ &p \in \check{P}, V_b^{eq} \in \nu_b^{eq}\} \end{aligned} \tag{18}$$

In second place, the following definition of robust stability is considered:

a) Definition: System (14) *is locally robustly stable if any equilibrium of the set $\chi^{eq}(P, \nu_b^{eq})$ is locally exponentially stable [32], [33].*

Then, from the above, to evaluate *Definition a)* from a reduced number of conditions, the following process is proposed. Firstly, the linearized system around a given x^{eq} is obtained by linearizing the nonlinear terms in system (14),

$$h_k = -\frac{p_k}{v_{bk}} \longrightarrow \left.\frac{p_k}{v_{bk}^2}\right|_{eq} v_{bk} \longrightarrow \Theta X \tag{19}$$

$$\dot{h}_k = \frac{d}{dt}(-\frac{p_k}{v_{bk}}) \longrightarrow 0\ in\ equilibrium \tag{20}$$

$$-\Delta r_k i_k \longrightarrow -I_k|_{eq}\,\Delta r_k\ -\Delta r_k|_{eq}\, i_k \longrightarrow -[\Upsilon + \Gamma]X \tag{21}$$

where $\Theta = \Theta(x^{eq})$, $\Upsilon = \Upsilon(x^{eq})$ and $\Gamma = \Gamma(x^{eq})$.

Then, the following system results:

$$\dot{z} = Az - M[\Upsilon + \Gamma]z + C\Theta z = A_z z \tag{22}$$

where $z(t) \in \Re^{4n}$ is the linearized state vector and $A_z = A - M.[\Upsilon + \Gamma] + C\Theta \in \Re^{4nx4n}$ is the system matrix.

Secondly, the set of system matrix $A_z = A_z(x^{eq})$ for a given set χ^{eq} is expressed in the form of a compact convex polytopic model. In order to do that and obtain a closed expression, the vertex representation given by the set of the vertices of the polytope is employed as:

$$A_z \in \Omega\ ,\ \Omega := \{A_z = \sum_{j=1}^{p} \xi_j \hat{A}_{zj}, \sum_{j=1}^{p} \xi_j = 1, \xi_j \geq 0\} \tag{23}$$

where the matrix $\hat{A}_{zj}$ is the j^{th} vertex of the set Ω and it can be determined by setting the uncertain terms in (22) in their extreme values:

$$\begin{aligned} &\hat{A}_{zj} = A - M[\Upsilon + \Gamma] + C\Theta \quad with \\ &\theta_k = \underline{\theta_k} = \frac{\underline{p_k}}{\overline{v_{bk}^{eq2}}} \quad or \quad \theta_k = \overline{\theta_k} = \frac{\overline{p_k}}{\underline{v_{bk}^{eq2}}},\ k = 1, ..., n \end{aligned} \tag{24}$$

where θ_k captures the overall uncertainty of p_k and v_{bk}^{eq}. In addition, I_k^{eq} and Δr_k^{eq} are determined by previously set variables values and equilibrium conditions x_{eq}.

Finally, to evaluate *Definition a)* over χ^{eq} is equivalent to analyze the stability of all the matrices in Ω. Furthermore,

since Ω is a polytopic set, any matrix $A_z \in \Omega$ can be expressed as convex combinations of the vertex matrices from $\hat{A}_{zj}$ according to the convex set theory. Then, it is a sufficient condition to only analyze the Hurwitz stability of all the vertex matrices $\hat{A}_{zj}$ to test the stability of all the matrices in Ω [32], [33].

IV. Results

A. Impact of load and power generation distribution

In the following, the presented model is applied to different scenarios of the same DCMG in order to evaluate the impact of variations in microgrid connections and the sensitivity to changes in the distribution of GNs and power loads. The 3-zones DCMG illustrated in Fig. 4 is considered with the parameters shown in Table I. The gains and parameters associated with the control were tuned by analyzing the small-signal block diagram corresponding to the local model of the individual units. Then, the transfer functions were calculated for a worst-case load and appropriate values of k_{pv}, k_{pi}, k_{iv}, k_{ii}, and r_{d0} were determined. To simplify the analysis without losing generality, these values were defined to be the same for all units.

Two cases are considered in this scenario: an unbalanced case, where the largest load is connected to the same unit as the smallest generation node, and a balanced case. These two cases are contrasted with a third scenario where the interconnection impedances are ignored. Then, this third scenario is equivalent to a single-PCC model where the equivalent load and all the GNs are connected to the same PCC, as shown in Fig. 5.

Fig. 6 shows the transient response of the bus voltages and output currents of the GNs obtained from circuital simulation using a Simulink (MatLab) environment. The circuital simulation involves two step variations in the power demanded by the CPL of each unit. At $t = 1\,\text{s}$, a change from zero load to a minimum load occurs, while at $t = 2\,\text{s}$, a second change takes place, bringing the loads to their maximum value.

On the one hand, in the first two scenarios, it can be observed that the voltage of the local DC buses converge

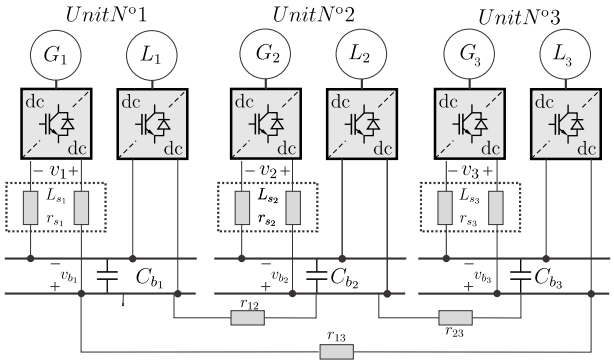

Fig. 4. Multi-unit representation of a 3-unit DCMG.

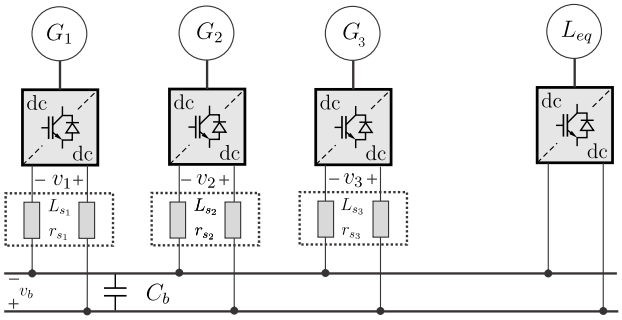

Fig. 5. Single-PCC representation of a 3-zone DCMG.

TABLE I
3-ZONE NETWORKING MG PARAMETERS

r_{s_1}	0.45Ω	r_{s_2}	0.525Ω	r_{s_3}	0.5Ω
L_{s_1}	1 mH	L_{s_2}	0.85 mH	L_{s_3}	1.15 mH
C_{b_1}	0.33 mF	C_{b_2}	0.5 mF	C_{b_3}	1 mF
r_{12}	2Ω	r_{23}	2Ω		
$I_{rate\ 1}$	10 A	$I_{rate\ 2}$	20 A	$I_{rate\ 3}$	30 A
r_{d0_1}	0.3	r_{d0_2}	0.15	r_{d0_3}	0.1
α_1	0.16	α_2	0.33	α_3	0.5
$\underline{V_{ref}}$	800 V	$\underline{V_{ref}}$	700 V		
$\overline{V_{MGref}}$	800 V	$\overline{V_{MGref}}$	700 V		
$k_{iv_k} = k_{ii_k}$	10	$k_{pv_k} = k_{pi_k}$	0.01		

Unbalanced Case

$\overline{p_1}$	70 kW	$\overline{p_2}$	$0.25\overline{p_1}$	$\overline{p_3}$	$0.1\ \overline{p_1}$
$\underline{p_1}$	1 kW	$\underline{p_2}$	1 kW	$\underline{p_3}$	1 kW
$\underline{v_{bk}}$	700 V	$\overline{v_{bk}}$	800 V		

Balanced Case

$\overline{p_1}$	$0.1\ \overline{p_3}$	$\overline{p_2}$	$0.25\ \overline{p_3}$	$\overline{p_3}$	70 kW
$\underline{p_1}$	1 kW	$\underline{p_2}$	1 kW	$\underline{p_3}$	1 kW
$\underline{v_{bk}}$	700 V	$\overline{v_{bk}}$	800 V		

Single-PCC Case

$\underline{p}$	3 kW	$\overline{p}$	94.5 kW
$\underline{v_{bk}}$	700 V	$\overline{v_{bk}}$	800 V

to different values, which is directly related to the current circulation among the different units and it is a needed situation to allow proportional load sharing among the GNs. In this regard, an unbalance distribution between the power generation and the demand lead to a greater current circulation through the interconnections, increasing the interaction among the GNs controllers and more abrupt voltage transients during the load steps. Moreover, it can be observed that the larger voltage drops are associated to the units with lower C_{b_k} values

TABLE II
3-UNIT NETWORKING MG OPERATION LIMITS

Method	Unbalanced Case	Balanced Case	Single-PCC Case
Simulation	$\overline{p}$ = 124 kW	$\overline{p}$ = 176.1 kW	$\overline{p}$ = 205 kW
Stability Analysis	$\overline{p}$ = 96.1 kW	$\overline{p}$ = 137 kW	$\overline{p}$ = 159.6 kW

and higher p_k values. Then, a more balanced distribution reduces the current circulation and coupling among the units allowing to switch larger loads. On the other hand, the third scenario shows a more relaxed situation, indicating that the conclusions drawn from this model are less conservative. Additionally, in all scenarios, it is noted that even though the instantaneous values of the DC bus voltages can exceed the steady-state minimum and maximum bounds, the voltage controllers successfully bring the global average voltage to the given setpoint.

These observations are confirmed with the obtained operation limits of the system, which are shown in Table II considering the proportions among p_1, p_2 and p_3 listed in I The process of determining the operation limit varies between the circuital simulation and the stability analysis. In the circuital simulation, the maximum power load is incrementally raised while maintaining all other parameters of the DCMG constant until the system reaches its limit, unable to handle a load step change from the minimum to the maximum load condition. On the other hand, in the stability analysis, the maximum power load is progressively increased while keeping all other DCMG parameters constant until the Hurwitz stability of any of the vertex system matrices $\hat{A}_{zj}$ is no longer maintained. Regarding the latter, Fig. 7 shows the eigenvalue locus for the three scenarios considered, i.e., the balanced, unbalanced, and single-PCC cases. Additionally, the graph is split into three frequency ranges to allow for clearer observation of the eigenvalues, and a zoomed section shows the detail of the eigenvalues close to the origin.

Regarding the results shown in Table II, it can be appreciated that the boundary operation condition are considerably different between the three scenarios, both as a result of the circuit simulation and the stability analysis presented. As a consequence, it can be stated that they do not correspond to equivalent situations. Secondly, and more importantly, it can be observed that the single-PCC representation turns unstable for larger loads and may lead the stability analysis to find an operating limit outside what the system can actually handle. In this case, the boundary operation condition obtained from the analysis applied to the single-PCC representation cannot be handle by the DCMG in an unbalanced scenario, meaning that the stability analysis is not conservative enough to completely disregard the information regarding power distribution in the microgrid. Otherwise, the conclusions reached by this representation require the definition of a security range. In this regard, comparing the curves shown in Fig. 6 and the eigenvalues shown in Fig. 7 it can be stated that the behaviour of the DCMG tends to the single-PCC scenario as the distribution balance is improved.

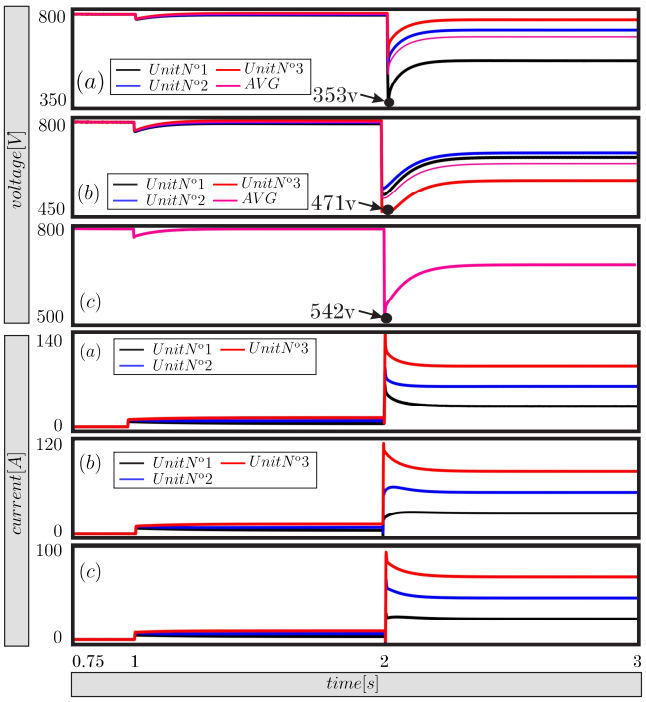

Fig. 6. Voltages and Currents transient response: (a) unbalanced case, (b) balanced case, (c) single-PCC model.

B. Stability analysis simulations

In this section, the presented analysis is employed to identify both, stable and unstable operation conditions, in the microgrid shown in Fig. 9, which is a more complex scenario and whose parameters are shown in Table III.

In Fig. 10, the eigenvalues of each unit (a total of 18) are presented for a stable operation condition. As in the previous section, the graph is split into three frequency ranges to allow a more clear observation of the eigenvalues. The main objective is to plot the variation of these eigenvalues between the extreme cases of operation, i.e, from the condition of minimum load and maximum voltage bus (represented by the $*$ symbols) to the maximum load and minimum voltage bus condition (represented by the o symbols). As can be seen in Fig. 10, the stability is ensured as all the eigenvalues of all vertex system matrix $\hat{A}_{zj}$ are Hurwitz stable. This result can be contrasted with a circuit simulation. In this sense, Fig. 8 shows the system response to the maximum load step given in Table III. As it can be observed, the DCMG remains stable after the load steps at $t = 0.5\,\mathrm{s}$ (minimum to maximum load) and at $t = 1.5\,\mathrm{s}$ (maximum to minimum load).

The presented analysis can be also applied to determine unstable load conditions. The procedure followed respects

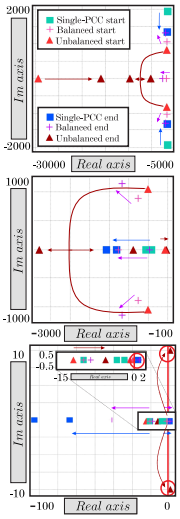

Fig. 7. Eigenvalues locus for the vertex matrices of balanced case, unbalanced case, and single PCC scenarios in the operation condition of Table II. Note that unstable eigenvalues have been highlighted by circling them in red.

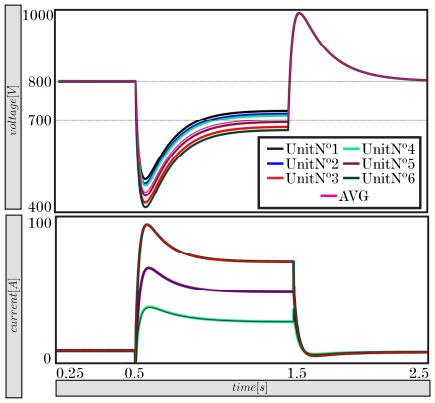

Fig. 8. Voltage and current transient response to maximum load steps.

what was indicated for the 3-unit DCMG scenario. In other words, the proportion between the six p_i of the microgrid is preserved as considered in Table III, while the total power load is increased until the system turns unstable. According to the presented analysis, stability is no longer ensured when some of the eigenvalues associated to $\hat{A}_{zj}$ shift to the right-half-plane. Fig. 11 shows the eigenvalues locus for this scenario. The limit value of total power resulting from the analysis is $\overline{p}$ = 200.2 kW, while the value obtained from circuit simulations turns to be $\overline{p}$ = 231 kW. In relation to the latter, as large signal stability is of interest, the system is considered to be unstable when it cannot handle a step change from the minimum load condition to the maximum load condition. Which is also the procedure followed for the 3-unit DCMG scenario. As it can be noted, the proposed model gives a conservative result due to the robust analysis inherent to the polytopic representation.

Finally, the presented formulation bases the condition of Hurwitz stability on the eigenvalues of the vertex matrices, allowing the analysis of the more suitable parameters to modify in order to improve the stability of the DCMG.

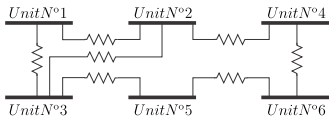

Fig. 9. DCMG case of study taken from [10].

TABLE III
6-ZONE NETWORKING MG PARAMETERS

r_{s_1}	0.45Ω	r_{s_2}	0.525Ω	r_{s_3}	0.5Ω
r_{s_4}	0.35Ω	r_{s_5}	0.25Ω	r_{s_6}	0.65Ω
L_{s_1}	1 mH	L_{s_2}	0.85 mH	L_{s_3}	1.15 mH
L_{s_4}	1 mH	L_{s_5}	0.85 mH	L_{s_5}	1.2 mH
C_{b_1}	0.33 mF	C_{b_2}	0.5 mF	C_{b_3}	1 mF
C_{b_4}	0.26 mF	C_{b_5}	0.47 mF	C_{b_6}	1 mF
$I_{rate\ 1}$	10A	$I_{rate\ 2}$	20A	$I_{rate\ 3}$	30A
$I_{rate\ 4}$	10A	$I_{rate\ 5}$	20A	$I_{rate\ 6}$	30A
r_{d0_1}	0.3	r_{d0_2}	0.15	r_{d0_3}	0.1
r_{d0_4}	0.3	r_{d0_5}	0.15	r_{d0_6}	0.1
α_1	0.083	α_2	0.167	α_3	0.246
α_4	0.083	α_5	0.167	α_6	0.246
$\overline{V_{ref}}$	800 V	$\underline{V_{ref}}$	700 V		
$\overline{V_{MGref}}$	800 V	$\underline{V_{MGref}}$	700 V		
$k_{iv_k} = k_{ii_k}$	10	$k_{pv_k} = k_{pi_k}$	0.01	r_{jk}	2Ω
$\overline{p_1}$	$0.1\overline{p_3}$	$\overline{p_2}$	$0.25\ \overline{p_3}$	$\overline{p_3}$	60 kW
$\overline{p_4}$	$0.26\ \overline{p_3}$	$\overline{p_5}$	$0.47\ \overline{p_3}$	$\overline{p_6}$	$1.0\ \overline{p_3}$
$\underline{p_1}$	1 kW	$\underline{p_2}$	1 kW	$\underline{p_3}$	1 kW
$\underline{p_4}$	1 kW	$\underline{p_5}$	1 kW	$\underline{p_6}$	1 kW
$\underline{v_{bk}}$	700 V	$\overline{v_{bk}}$	800 V		

To conduct this analysis, the DCMG shown in Fig. 9 is taken to the critical load condition found in the previous paragraph. Then, a small perturbation is made over different parameters of the DCMG, and the variation in the value of the critical eigenvalue (i.e., the one that turns unstable sooner) is calculated. Fig. 12 presents a summary of the results obtained for the percentage variation of the critical eigenvalue. The calculation was performed using the following expression:

$$Variation[\%] = \frac{\frac{e_{final}-e_{initial}}{e_{initial}}}{\frac{Parameter_{final}-Parameter_{initial}}{Parameter_{initial}}}100\% \tag{25}$$

where the numerator is the relative eigenvalue variation and the denominator is the relative parameter variation. From the given expression, it is evident that a negative percentage variation indicates that the eigenvalue moves towards the left-half-plane, i.e., towards a stable condition. Conversely, a positive percentage variation indicates the opposite, suggesting

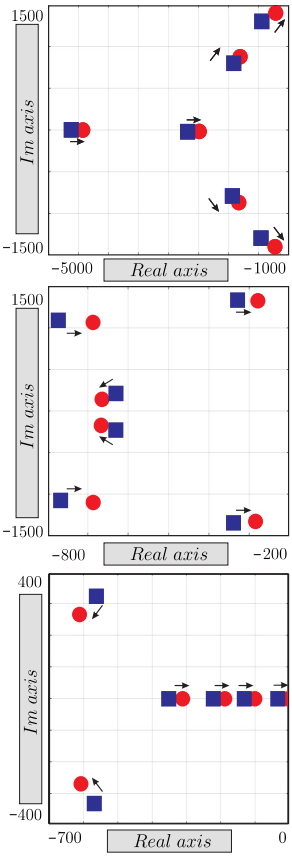

Fig. 10. Eigenvalues locus for the vertex matrices in a stable scenario.

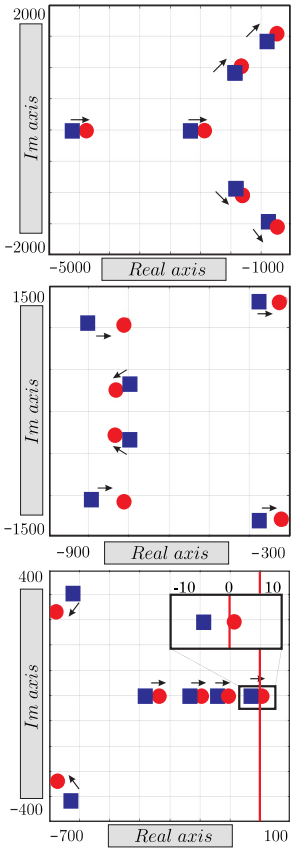

Fig. 11. Eigenvalues locus for the vertex matrices in a unstable scenario.

a movement away from the stable condition.

The analysis was conducted both individually for each unit parameter, as shown in the first n bars of each subplot in the figure, and by simultaneously modifying the value for all units, represented by the last bar of each subplot. In the last subplot, the last bar specifically demonstrates the impact of modifying the base droop resistance value (r_{d0}). Based on the obtained results, several observations can be made:

- Increasing the gains associated with the voltage controller (k_{iv_k}, k_{pv_k}) leads to a beneficial variation.
- Increasing the gains associated with the current controller (k_{ii_k}, k_{pi_k})leads to a detrimental variation.
- Changing the current distributions, which are determined by the ratios of the I_{rate_k}, leads to a more beneficial variation when they generate a more equitable distribution among the GNs or they force the GNs associated with the more demanding loads to contribute with most part of the total load.
- Changing the base value of the droop resistance r_{d0} has almost no impact.

Therefore, some insights can be made. The convergence of the DC bus voltage to its reference value is a priority over the convergence of the output currents if stability needs to be improved. The adaptive term Δr_k dominates the term r_{d0} in determing the system stability, turning the tuning of the static value less important. It is important to note that the analysis is based on a small variation of the studied parameters, and these observations may not be valid for larger variations. For instance, larger increases in the values of the k_{iv_k} can turn a secondary eigenvalue unstable. Therefore, when making larger variations, the tuning process must consider the impact on the rest of the eigenvalues.

V. Conclusions

In this paper, a stability analysis for networking DCMGs with distributed control and uncertain CPLs was presented. In this sense, the concept of convex polytopic sets allowed to represent the uncertain time-varying nature of the loads and obtain a set of sufficient conditions to evaluate the stability of the system under a robust approach. According to the correlation between the load power limits obtained from circuit simulation and the presented analysis, it can be stated that the analysis correctly determines stable operation and returns conservative results regarding the limit operation conditions that keep the system stable, which is a typical feature of robust analysis approaches. Additionally, the results highlighted different representations of a same DCMG can lead to different conclusions, and, consequently, information regarding units interconnection and distributions of GNs and loads cannot be completely disregarded. Lastly, the Hurwitz stability criteria, based on the eigenvalues locus, provided valuable insight for a more comprehensive interpretation of the impact of the DCMG parameters on the system stability.

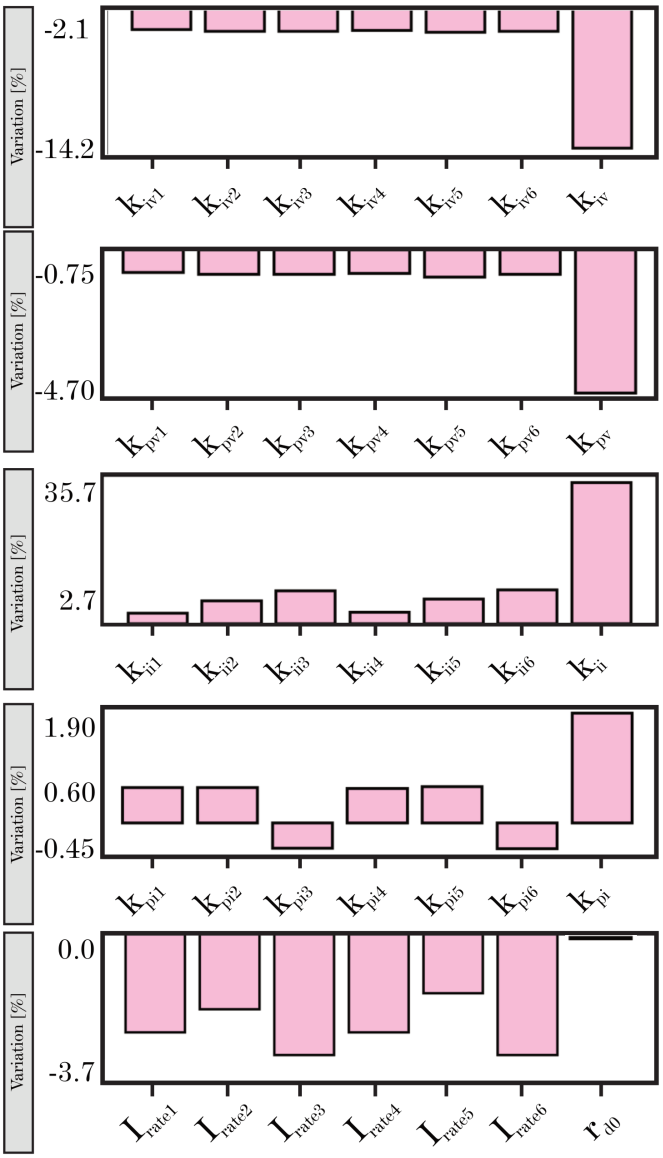

Fig. 12. Bar graph showing the impact of different parameters of the DCMG on the critical eigenvalue, with each bar representing the variation produced by a specific parameter. The results indicate the relative importance of each parameter in improving the stability of the DCMG.

This advantage was employed to evaluate which modifications of the controller's gains and parameters are more beneficial in improving the stability of the system under a critical load condition.

REFERENCES

[1] T. Dragicevic, X. Lu, J. C. Vasquez, and J. M. Guerrero, "Dc microgrids—part i: A review of control strategies and stabilization techniques," *IEEE Trans. Power Electron.*, vol. 31, no. 7, pp. 4876–4891, 2016.

[2] T. Dragicevic, J. C. Vasquez, J. Guerrero, and D. Skrlec, "Advanced lvdc electrical power architectures and microgrids: A step toward a new generation of power distribution networks.," *Electrification Magazine, IEEE*, vol. 2, pp. 54–65, 03 2014.

[3] J. M. Rey, G. A. Vera, P. Acevedo-Rueda, J. Solano, M. A. Mantilla, J. Llanos, and D. Sáez, "A review of microgrids in latin america: Laboratories and test systems," *IEEE Latin America Transactions*, vol. 20, p. 1000–1011, Feb. 2022.

[4] K. M. Bhargavi, N. S. Jayalakshmi, D. N. Gaonkar, A. Shrivastava, and V. K. Jadoun, "A comprehensive review on control techniques for power management of isolated dc microgrid system operation," *IEEE Access*, vol. 9, pp. 32196–32228, 2021.

[5] X. Lu, J. Guerrero, K. Sun, and J. C. Vasquez, "An improved droop control method for dc microgrids based on low bandwidth communication with dc bus voltage restoration and enhanced current sharing accuracy," *IEEE Trans. Power Electron.*, vol. 29, pp. 1–12, 01 2013.

[6] V. Nasirian, A. Davoudi, F. L. Lewis, and J. M. Guerrero, "Distributed adaptive droop control for dc distribution systems," *IEEE Trans. Energy Convers.*, vol. 29, no. 4, pp. 944–956, 2014.

[7] H. Kakigano, Y. Miura, and T. Ise, "Low-voltage bipolar-type dc microgrid for super high quality distribution," *Power Electronics, IEEE Transactions on*, vol. 25, pp. 3066 – 3075, 01 2011.

[8] T. Dragicevic, X. Lu, J. C. Vasquez, and J. Guerrero, "Dc microgrids–part ii: A review of power architectures, applications and standardization issues," *IEEE Transactions on Power Electronics*, vol. 31, pp. 3528–3549, 01 2015.

[9] J.-D. Park, J. Candelaria, L. Ma, and K. Dunn, "Dc ring-bus microgrid fault protection and identification of fault location," *Power Delivery, IEEE Transactions on*, vol. 28, pp. 2574–2584, 10 2013.

[10] C. Li, F. de Bosio, S. K. Chaudhary, M. Graells, J. C. Vasquez, and J. M. Guerrero, "Operation cost minimization of droop-controlled dc microgrids based on real-time pricing and optimal power flow," in *IECON 2015 - 41st Annual Conference of the IEEE Industrial Electronics Society*, pp. 3905–3909, 2015.

[11] L. Che and M. Shahidehpour, "Dc microgrids: Economic operation and enhancement of resilience by hierarchical control," *IEEE Transactions on Smart Grid*, vol. 5, no. 5, pp. 2517–2526, 2014.

[12] Z. Xu, P. Yang, C. Zheng, Y. Zhang, J. Peng, and Z. Zeng, "Analysis on the organization and development of multi-microgrids," *Renewable and Sustainable Energy Reviews*, vol. 81, pp. 2204–2216, 2018.

[13] D. Kumar, F. Zare, and A. Ghosh, "Dc microgrid technology: System architectures, ac grid interfaces, grounding schemes, power quality, communication networks, applications and standardizations aspects," *IEEE Access*, vol. 5, pp. 12230–12256, 04 2017.

[14] L. Che, X. Zhang, and M. Shahidehpour, "Resilience enhancement with dc microgrids," in *2015 IEEE Power & Energy Society General Meeting*, pp. 1–5, 2015.

[15] Z. Li, M. Shahidehpour, F. Aminifar, A. Alabdulwahab, and Y. Al-Turki, "Networked microgrids for enhancing the power system resilience," *Proceedings of the IEEE*, vol. 105, no. 7, pp. 1289–1310, 2017.

[16] M. Shahidehpour and M. Khodayar, "Cutting campus energy costs with hierarchical control: The economical and reliable operation of a microgrid," *Electrification Magazine, IEEE*, vol. 1, pp. 40–56, 09 2013.

[17] A. P. N. Tahim, D. J. Pagano, E. Lenz, and V. Stramosk, "Modeling and stability analysis of islanded dc microgrids under droop control," *IEEE Trans. Power Electron.*, vol. 30, no. 8, pp. 4597–4607, 2015.

[18] M. Kabalan, P. Singh, and D. Niebur, "Large signal lyapunov-based stability studies in microgrids: A review," *IEEE Transactions on Smart Grid*, vol. 8, no. 5, pp. 2287–2295, 2017.

[19] M. H. Saeed, W. Fangzong, B. A. Kalwar, and S. Iqbal, "A review on microgrids' challenges & perspectives," *IEEE Access*, vol. 9, pp. 166502–166517, 2021.

[20] J. Elizondo, R. Y. Zhang, J. K. White, and J. L. Kirtley, "Robust small signal stability for microgrids under uncertainty," in *2015 IEEE 6th International Symposium on Power Electronics for Distributed Generation Systems (PEDG)*, pp. 1–8, 2015.

[21] L. Herrera, W. Zhang, and J. Wang, "Stability analysis and controller design of dc microgrids with constant power loads," *IEEE Transactions on Smart Grid*, vol. 8, no. 2, pp. 881–888, 2017.

[22] N. Yang, F. Gao, D. Paire, A. Miraoui, and w. liu, "Distributed control of multi-time scale dc microgrid based on adrc," *IET Power Electronics*, vol. 10, 10 2016.

[23] X. Lu, K. Sun, J. M. Guerrero, J. C. Vasquez, L. Huang, and J. Wang, "Stability enhancement based on virtual impedance for dc microgrids with constant power loads," *IEEE Transactions on Smart Grid*, vol. 6, no. 6, pp. 2770–2783, 2015.

[24] D. Liu, K. Jiang, L. Yan, X. Ji, K. Cao, and P. Xiong, "A fully distributed economic dispatch method in dc microgrid based on consensus algorithm," *IEEE Access*, vol. 10, pp. 119345–119356, 2022.

[25] S. Chen, Q. Gong, X. Lu, and J. Lai, "Distributed cooperative control for economic dispatch and soc balance in dc microgrids with vanadium redox batteries," *Sustainable Energy, Grids and Networks*, vol. 28, p. 100534, 2021.
[26] J. Liu, W. Zhang, and G. Rizzoni, "Robust stability analysis of dc microgrids with constant power loads," *IEEE Transactions on Power Systems*, vol. 33, no. 1, pp. 851–860, 2018.
[27] R. Brigham and R. Dutton, "On neighborhood graphs," *Journal of Combinatorics, Information & System Sciences*, vol. 12, 01 1987.
[28] T. Vu, D. Perkins, F. Diaz, D. Gonsoulin, C. Edrington, and T. El-mezyani, "Robust adaptive droop control for dc microgrids," *Electric Power Systems Research*, vol. 146, 01 2017.
[29] M. Mokhtar, M. I. Marei, and A. A. El-Sattar, "An adaptive droop control scheme for dc microgrids integrating sliding mode voltage and current controlled boost converters," *IEEE Transactions on Smart Grid*, vol. 10, no. 2, pp. 1685–1693, 2019.
[30] K. Gu, V. Kharitonov, and J. Chen, *Stability of Time-Delay Systems*. New York: Springer, 2003.
[31] Y. He, M. Wu, J.-H. She, and G.-P. Liu, "Parameter-dependent lyapunov functional for stability of time-delay systems with polytopic-type uncertainties," *IEEE Transactions on Automatic Control*, vol. 49, no. 5, pp. 828–832, 2004.
[32] P. Gahinet, P. Apkarian, and M. Chilali, "Affine parameter-dependent lyapunov functions and real parametric uncertainty," *IEEE Trans. Autom. Control*, vol. 41, no. 3, pp. 436–442, 1996.
[33] M. Mansour, "Sufficient conditions for the asymptotic stability of interval matrices," *International Journal of Control*, vol. 47, no. 6, pp. 1973–1974, 1988.